Design and Control of a New Wrist Rehabilitation Robot

Simona-Daiana Stiole¹ ¹ ¹ ⁰ Pusca Alexandru¹ ¹ Paul Tucan¹ ¹ ⁰, Iuliu Nadas¹ ⁰, Vasile Bulbucan¹ ⁰ Andrei Cailean lof, Dragos Sebeni log, Alexandru Banica loh, Daniela Jucan loi, Radu Morariu loj, Calin Vaida¹ Ok, Petru Dobra Obra Machado^{1,2} Om and Doina Pisla^{1,3} On

 1 CESTER Research Center for Industrial Robots Simulation and Testing, Technical University of Cluj-Napoca, Memorandumului 28, 400114 Cluj-Napoca, Romania

²MEtRICs Research Center, Campus of Azurém, University of Minho, 4800-058, Guimarães, Portugal ³Technical Sciences Academy of Romania, B-dul Dacia, 26, 030167, Bucharest, Romania {simona.sim, petru.dobra}(c dragos.sebeni, radu.ı

Keywords: Wrist Rehabilitation Robot, Robot Design, Kinematic, Dynamic Model, Cost-Effective Robotic,

Tracking Control.

Abstract: This paper presents the design and control of a cost-effective wrist rehabilitation robot with the aim of providing an accessible and scalable solution for patients in need of upper-limb motor recovery. The primary goal is to create a compact system that can support repetitive and controlled wrist movements, particularly for

individuals recovering from stroke. The robot's mechanical structure, forward kinematic model and dynamic model were defined to minimize cost without compromising essential therapeutic functionality. Three control strategies were implemented and evaluated in simulation, including Independent Joint Control, Linear Quadratic Regulator, and an observer-based version using a Luenberger estimator for situations where only position sensors are available. These simulations serve to assess the feasibility of each control method in terms

of performance, complexity, and compatibility with low-cost components for future hardware development.

INTRODUCTION

The use of robotic systems in physical rehabilitation, particularly for upper-limb therapy (Pollock, et al., 2014), (Basteris, et al., 2014), (Tucan, et al., 2022), (Tohanean, et al., 2023), has seen substantial growth in recent years. Robotic devices (Guozheng, et al., 2014) for wrist rehabilitation are increasingly being incorporated into therapy programs (Wu Chuang, et al., 2011) due to their ability to deliver consistent, repetitive, and quantifiable movements - crucial factors in the recovery of fine motor skills. Several commercially available systems, such as MIT-Manus

(Krebs, et al., 1999), WristBot (Squeri, et al., 2014), or Reharob (Toth, et al., 2005), have demonstrated the feasibility of robotic-assisted therapy for post-stroke (Parisi, et al., 2022) patients. These systems generally employ complex mechanical structures and control algorithms, such as impedance control, adaptive control, or model predictive control, to guide patient movement. However, many solutions come with significant trade-offs in terms of cost, size, and system complexity (Akdogan, 2016), which limit their accessibility outside specialized clinical environments. Moreover, a large part of the literature focuses on multi-DOF exoskeletons (Vaida, et al., 2018) or hybrid systems, which may be excessive for

^a https://orcid.org/0009-0002-5062-6936

^b b https://orcid.org/0000-0002-5804-575X

^c https://orcid.org/0000-0001-5660-8259

d **b** https://orcid.org/0000-0002-6722-9972

e https://orcid.org/0009-0005-3867-7687

f b https://orcid.org/0009-0004-4758-0468

g b https://orcid.org/0009-0009-7615-6240

h https://orcid.org/0000-0001-7781-342X

i https://orcid.org/0009-0004-0219-9858

j https://orcid.org/0000-0003-4216-6132

k https://orcid.org/0000-0003-2822-9790

¹ https://orcid.org/0000-0001-6041-5820

m b https://orcid.org/0000-0002-4917-2474

ⁿ https://orcid.org/0000-0001-7014-9431

specific rehabilitation needs such as isolated wrist joint therapy. As noted in (Omarkulov, et al., 2016), simpler, task-specific devices can often achieve comparable outcomes if paired with efficient control strategies, while also being more adaptable to homebased therapy. The study in (Masiero, et al., 2011) demonstrates that early robot-assisted therapy can significantly improve upper-limb motor recovery in stroke patients. The present work proposes a costeffective robotic solution dedicated to wrist rehabilitation. Additionally, unlike the NeReBot (Rosati, et al., 2007) trial which centers on clinical protocol evaluation, this paper focuses on the comparison of three control strategies 1) Independent Joint Control (IJC), 2) Linear Quadratic Regulator (LOR), and 3) Luenberger observer-based LOR controller - highlighting how different control methods impact performance, robustness, and the feasibility of developing rehabilitation devices.

Therefore, this paper proposes a new wrist rehabilitation robot, with a focus on simplicity, compactness, and cost-efficiency, aiming to provide accessible therapeutic support for patients in need of upper-limb motor recovery. The device is developed to allow repetitive and controlled wrist movements, such as flexion and extension (Major, et al., 2021), (Tarnita, et al., 2022), which are commonly required in post-stroke.

To evaluate the feasibility of various control solutions for such a system, three strategies were implemented and tested in simulation. IJC was considered as a baseline method, leveraging its simplicity and ease of implementation. A more advanced approach based on linearization followed by LQR control was also explored, enabling better tracking performance and disturbance rejection by accounting for system nonlinearities. In addition, a Luenberger observer was integrated to estimate the full state vector in scenarios where only joint position measurements are available - a common situation in low-cost hardware implementations. Even if additional sensors are introduced, they are likely to be low-cost and less accurate, which would require further filtering and increase system complexity.

To enable effective and affordable wrist rehabilitation solutions, this study investigates three control strategies implemented on a custom-designed robotic platform. Each method offers distinct advantages, making them suitable for different application contexts. In particular, the LQR + Observer demonstrates strong potential for maintaining control performance while reducing sensor requirements, addressing a challenge in the development of low-cost rehabilitation devices. It

also investigates whether control performance can still be maintained using lightweight design and standard components - without sacrificing precision. The findings will guide future development of accessible robotic therapy platforms that balance performance, cost, and usability.

This paper is organized as follows: Section 2 presents the mechanical design of the wrist rehabilitation robot, outlining its purpose, intended use, and functional relevance. This section also includes the forward kinematic and dynamic model of the system. Section 3 introduces three control strategies - 1) IJC, 2) LQR, and 3) Luenberger observer-based LQR controller - each discussed with respect to its specific advantages and applicability. In Section 4, the simulation results obtained using these control methods are analysed. Finally, Section 5 summarizes the main conclusions of the study and outlines directions for future development.

2 ROBOT DESIGN AND DYNAMIC MODELING

The robot proposed within this paper (WRIST-X) is a novel 3-DOF rehabilitation robot, able to perform flexion, extension, adduction, abduction, pronation and supination of the wrist (Mehrez, et al., 2025). The main wrist rehabilitation movements targeted in this study are flexion/extension, adduction/abduction, and pronation/supination.

The virtual model of the rehabilitation robot is presented in Figure 2. The final prototype can be seen in Figure 3. The robot has 5 major components: the forearm rest responsible for anchoring the arm of the patient in such manner that the centre of the wrist joint falls at the intersection point of the robot's motion axis (point O). The adduction/abduction mechanism performs the revolute motion around the OZ axis, the flexion/extension mechanism performs revolute motion the axis around OY and the pronation/supination mechanism performs revolute motion around the OX axis. During the rehabilitation procedure the patient grabs the handle of the robot and all the rehabilitation motions are performed with the closed fist.

Basically, the robot consists of three revolute joints performing the rehabilitation motions individually and several adjustment passive/lockable mechanisms to allow the configuration of the robot to comply to different anthropometric characteristics of the patient.

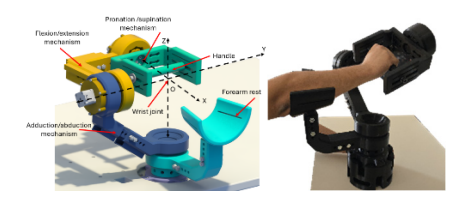


Figure 1: Design and prototype of the robot.

The joint angles are denoted as:

$$q_1 = \psi, q_2 = \theta, q_3 = \varphi \tag{1}$$

where q₁, q₂, q₃ represent the active joints of the mechanism, ψ represents the adduction/abduction angle, θ represents the flexion/extension angle and φ represents the pronation/supination angle.

The explicit rotation matrix of the system is obtained as:

$$R = R_x(\varphi)R_y(\theta)R_z(\psi) \tag{2}$$

where R_x , R_y , R_z are standard rotation on x/y/z-axis, (Spong, Hutchinson, & Vidyasagar, 2005) matrices.

The angular velocity expressed in the space frame is computed using (4):

$$\vec{\omega} = J(q) \cdot \dot{q} \tag{3}$$

where
$$J(q) = \begin{bmatrix} 0 & \cos \psi & \cos \psi \cos \theta \\ 0 & \sin \psi & \sin \psi \cos \theta \\ 1 & 0 & -\sin \theta \end{bmatrix}$$
 denotes the Jacobian. The accelerations are determined as:

$$\vec{\alpha} = J(q) \cdot \dot{q} + J(q)\ddot{q} \tag{4}$$

where:

$$\dot{J}(q) = \begin{bmatrix}
0 & -\sin\psi\dot{\psi} & -\sin\psi\cos\theta\dot{\psi} - \cos\psi\sin\theta\dot{\theta} \\
0 & \cos\psi\dot{\psi} & \cos\psi\cos\theta\dot{\psi} - \sin\psi\sin\theta\dot{\theta} \\
0 & 0 & -\cos\theta\dot{\theta}
\end{bmatrix} (5)$$

To implement and validate control strategies, a dynamic model of the system is necessary. For this robot, the wrist joint dynamics can be approximated using the classical Euler-Lagrange modelling approach (Spong, et al., 2005).

The dynamic modelling of the robot was performed by excluding the detailed characteristics of the motors. The torque and power requirements were estimated independently of motor dynamics to evaluate the suitability of different motor types for achieving the desired performance. Additionally, frictional effects were neglected at this stage to simplify the model and focus on the core mechanical dynamics. These assumptions serve as a preliminary step in the design process, with the understanding that motor behaviour and friction will be incorporated in future developments for more accurate simulation

and control. The general equation of motion for an ndegree of freedom (DOF) manipulator is given by:

$$D(q)\ddot{q} + C(q,\dot{q})\dot{q} + G(q) = \tau \tag{6}$$

where $q \in \mathbb{R}^n$ is the vector of generalized joint coordinates, \dot{q} , \ddot{q} are the joint velocities and accelerations, $D(q) \in \mathbb{R}^{n \times n}$ is the inertia matrix, $C(q, \dot{q}) \in \mathbb{R}^{n \times n}$ is the Coriolis and centrifugal matrix, $G(q) \in \mathbb{R}^n$ is the gravity vector and $\tau \in \mathbb{R}^n$ is the vector of applied joint torques.

For the wrist rehabilitation robot presented in this paper, the configuration consists of three rotational DOF (i.e. n = 3). The parameters of the model, such as link masses, lengths, and moments of inertia, were defined based on the mechanical design using the 3D virtual model designed using Siemens NX.

The matrices in (8) are:

$$D = \begin{pmatrix} d_1 - d_2 \cdot (s(2))^2 & d_3 \cdot s(2) & -d_4 \cdot s(2) \\ d_3 \cdot s(2) & d_5 & 0 \\ -d_4 \cdot s(2) & 0 & d_4 \end{pmatrix}$$

where $d_1 = 0.088$, $d_2 = 0.006$, $d_3 = 0.034$, $d_4 =$ $0.0027, d_5 = 0.0209, \ s(i) = \sin(q_i), c(i) =$ $\cos(q_i)$, $i = \overline{1,3}$.

$$C = \begin{pmatrix} -\dot{q}_2(2c_1 s(2) c(2)) & 0 & 0\\ 0 & c_2 \cdot \dot{q}_1 \cdot c(2) & c_3 \cdot q_1 \cdot c(2)\\ 0 & c_3 \cdot q_1 \cdot c(2) & 0 \end{pmatrix}$$
where $c_1 = 0.0031, c_2 = 0.0339, c_3 = -0.00135$

 $G = (0, 1.3029 \cdot c(2), 0)^T$.

The dynamic model provides the base for the control strategies in the following sections and allows for torque estimation necessary for future motor selection. In addition, a saturation limit of $+10 N \cdot m$ was applied to the control input to reflect the limitations of the motors, for ensuring that the simulated control efforts remain within realistic actuator capabilities.

CONTROL STRATEGIES

Three control approaches (output feedback and state feedback) for wrist rehabilitation robots, were developed and tested in simulation. The control strategies feed into a microprocessor. The microprocessor communicates bidirectionally with a user interface that allows a therapist to monitor, evaluate, and adjust treatment parameters in real time. Simultaneously, the microprocessor sends commands to three DC motors that drive the robotic arm. The robotic arm, in contact with the patient, performs therapeutic movements. Feedback from the robot is

captured by encoders and sensors. This feedback is relayed back to the microprocessor to adjust control outputs dynamically, ensuring tracking position.

All control strategies presented in this work were initially designed and applied to the linearized model of the system, and their performance was subsequently validated by testing them on the full nonlinear model. Starting from the dynamic model (6) we want to achieve the linearized form:

$$\dot{x} = \begin{bmatrix} \dot{x}_a \\ \dot{x}_b \end{bmatrix} = \begin{bmatrix} f_a \\ f_b \end{bmatrix}; f_a = x_b$$

$$f_b = \ddot{q} = D^{-1}(q)(\tau - C(q, \dot{q})\dot{q} - G(q))$$
(7)

where $x_a = [q_1, q_2, q_3]^T$ represents the positions and $x_b = [\dot{q}_1, \dot{q}_2, \dot{q}_3]^T$ the velocities.

Following the linearization of the nonlinear dynamic model, the system was reduced to a linear, controllable it is an double integrator for each joint vector considering the state $[q_1, q_2, q_3, \dot{q}_1, \dot{q}_2, \dot{q}_3]^T$. The system was linearized around the equilibrium point $x_0 = [0, 0, 0, 0, 0, 0]^T$ and $u_0 = \tau_0 = [0, 1.3029, 0]^T$ which represents the wrist being at rest in the neutral (horizontal) position.

The resulting system is controllable and is described below:

$$\dot{x} = A \cdot x + B \cdot \underline{\Delta} u
y = C \cdot x + D \cdot \underline{\Delta} u$$
(8)
$$A = \begin{pmatrix} O_3 & I_3 \\ O_3 & O_3 \end{pmatrix}; C = (I_3 & O_3); D = O_3$$
(9)
$$B = \begin{pmatrix} 0 & 0 & 0 \\ 0 & 0 & 0 \\ 0 & 0 & 0 \\ 11.41 & 0 & 0 \\ 0 & 47.84 & 0 \\ 0 & 0 & 370.37 \end{pmatrix}$$
(10)

(8)

where x is the state vector (joint positions and velocities), $\Delta u = u - u_0$ is the control input vector (joint torques). O_3 denotes the 3x3 zero matrix, and I_3 represents the 3x3 identity matrix.

The first method implemented was IJC (Spong, et al., 2005), a straightforward strategy based on classical PID, commonly used for systems with minimal coupling and well-understood dynamics.

Subsequently, an optimal control strategy - the LQR (Spong, et al., 2005) was implemented, improving tracking performance and disturbance rejection by explicitly accounting for the system's state and optimizing control effort.

Finally, to address the practical limitation of not having full state measurement in real-world applications, a Luenberger observer (Levine, 2011) was designed and implemented to estimate

unmeasured state variables (e.g., angular velocity) based on available position feedback.

Independent Joint Control (IJC)

IJC is one of the most intuitive and widely used control strategies in robotics, especially when dealing with systems where dynamic coupling between joints is minimal (Spong, et al., 2005) or deliberately neglected. Given the nature of the rehabilitation robot, the IJC approach is suitable and provides a baseline for performance evaluation.

In this method, each joint q_i is controlled separately, typically using a Proportional-Derivative (PD: $K_p + K_d \cdot s$) controller as it can be seen in Figure 2 where q_{di} is the desired reference value. The simplified model assumes the robot behaves like a second-order system with torque input and angular position output.

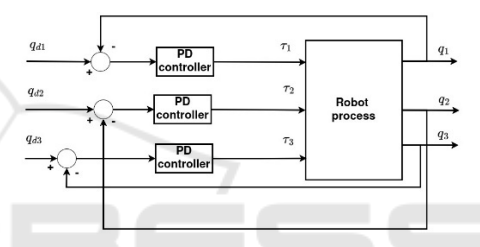


Figure 2: Control structure for IJC.

This method is advantageous due to its ease of and minimal computational implementation requirements. However, it does not take into account nonlinearities or external disturbances explicitly, and performance may degrade in scenarios involving interaction with a variable load (Prewett, at al., 2010) (e.g., patient effort during therapy). The IJC strategy (Spong, et al., 2005) starts from the idea of simplifying the nonlinear, coupled dynamics of the robot by reducing it to a set of three decoupled second-order linear systems. This is achieved by treating the dynamic interactions between joints and other nonlinear effects as external disturbances. Once the system is expressed in this simplified second order (11) form for each joint, the control design proceeds by imposing the denominator of the closedloop (13) performance specifications directly.

$$s^2 + 2\zeta\omega_n s + \omega_n^2 \tag{11}$$

Specifically for our robot, the desired damping ratio $\zeta=1$ and natural frequency $\omega_n=10 \ rad/sec$ are selected to define the transient behavior, such as small settling time and no overshoot.

The closed-loop transfer function results:

$$H(s) = \frac{K_{di} \cdot K_{qi} \cdot s + K_{pi} \cdot K_{qi}}{s^2 + K_{di} \cdot K_{ai} s + K_{pi} \cdot K_{ai}}$$
(12)

The resulting control law is:

$$\tau_i(t) = K_{p_i} \cdot e_i(t) + K_{d_i} \cdot \dot{e}_i(t) \tag{13}$$

where e(t) is the position tracking error, K_p is the proportional gain, K_d is derivative gain of the controller, $K_q = [11.4; 47.84; 370.37]$ is the proportional constant of the individual transfer function for each joint and $i = \overline{1,3}$ corresponding to the joint position.

By matching the characteristic equation of the closed-loop system (12) to the standard second-order form (11), the controller gains are computed analytically. In practice, the choice of ω_n is limited by the physical constraints of the system, particularly actuator saturation. Therefore, the highest feasible ω_n is selected to balance performance and input limitations. This allows the designer to systematically tune the controller based on clear performance objectives that can be easily implemented on each joint q_i (i.e. $i = \overline{1,3}$) independently.

3.2 LQR Control

To enhance control performance, particularly in terms of precision and energy efficiency, a Linear Quadratic Regulator (LQR) (Levine, 2011) is considered.

The LQR control law is given by:

$$u(t) = -Kx(t) + u_0 \tag{14}$$

where u(t) is the input, x(t) is the state vector of the system and K is the optimal gain matrix computed to minimize the quadratic cost function:

$$J = \int_0^\infty (x^T Q x + u^T R u) dt \tag{15}$$

where $Q \in \mathbb{R}^{6 \times 6}$ and $R \in \mathbb{R}^{3 \times 3}$ are symmetric positive semi-definite matrices that penalize deviations, respectively the control effort.

The tracking problem in LQR is defined as the requirement for the system output to follow a given reference trajectory q_r . Specifically, the position tracking error, defined as $q_r - q$ must converge to zero. The reference state vector x_r is defined to include the desired joint positions q_r and corresponding zero velocities, resulting in $x_r = [q_r, 0]^T$. The control law is then applied in the form:

$$u(t) = -K(x(t) - x_r(t)) + u_0 \tag{16}$$

where u_0 corresponds to the equilibrium condition used during the linearization process.

3.3 State Estimation

In practical applications, it is often not feasible to measure all state variables directly due to sensor limitations or cost constraints. To enable the implementation of state-feedback control, it is therefore necessary to estimate the full state vector from the available measurements. To this end, a Luenberger observer was designed based on the linearized model of the system, following the methodology described in (Levine, 2011) and applied on the nonlinear process. The observer reconstructs the unmeasured states by using the system's model and correcting the estimation based on the error between the measured and estimated outputs.

The linear observer has the following structure:

$$\dot{x_e}(t) = A \cdot x_e + B \cdot u + L(y(t) - y_e(t)) \tag{17}$$

After computing L, the nonlinear observer is:

$$\dot{x_e}(t) = f(x_e, u) + L(y(t) - y_e(t)) \tag{18}$$

where $x_e(t)$ is the estimated state vector, $f(x_e, u)$ represents the nonlinear system as presented in (7), L is the observer gain matrix designed for the linear model, y(t) is the measured output (in this case, joint position) and $y_e(t) = Cx_e(t)$ is the estimated output.

4 RESULTS

evaluate the performance of the implemented control strategies - 1) IJC, 2) LQR, 3) LQR and Luenberger observer - simulations were conducted in Matlab/Simulink using the previously defined dynamic model in (8). All the results are presented for the nonlinear system, with white measurement noise added to the joint position signals to simulate realistic sensing conditions. The evaluation focused on trajectory tracking performance (x_1 for adduction and abduction motion, x_2 for flexion and extension motion and x_3 for pronation and supination motion), disturbance rejection, and control effort.

The initial conditions were set to $x_0 = [0.3, -0.3, 0.4, 0, 0, 0]^T$ and the reference position is $x_r = [-0.2, -0.1, -0.2, 0, 0, 0]^T$.

Following the tuning guidelines mentioned above, the controller gains used for the joints in the IJC approach are $K_p = [8.76, 2.09, 0.001], K_d = [1.75, 0.41, 0.0001].$

These values were found to provide acceptable tracking performance and stable response for the desired reference. Figure 3 illustrates the response of

the system states under the IJC strategy, alongside the reference signals (with red colour - the reference and with blue - the joints positions). The measured settling times are approximately 0.64 sec for joint x_1 , 0.7 sec for joint x_2 , and significantly lower at 0.3 sec for joint x_3 . A small steady-state position error of approximately is present for joint x_3 , indicating the limitations of this decoupled control approach in fully compensating for system nonlinearities and interactions. Additionally, an overshoot was observed for joint x_2 . Despite these limitations, the controller maintains stable behaviour across all joints, making it a viable solution for applications where cost and simplicity are prioritized over high precision.

Moving to LQR simulations, combinations of Q and R (Franklin, et al., 2014) were tested through iterative tuning using the linearized system to identify a configuration that provides a balance between control effort, settling time, overshoot, and tracking accuracy. Lower values in R favor aggressive control with faster response, while higher weights in Q emphasize precise state tracking. Higher weights were assigned to the position states in matrix Q to prioritize trajectory tracking, while lower weights were set for the velocity states to reduce sensitivity to noise and avoid aggressive control actions. The final selected values achieved smooth and accurate tracking with moderate control inputs, the controller viable for real-time implementation. The chosen configuration is also suitable for low-cost implementations, as it does not require high-speed computation or complex hardware resources. The final values for Q, R and K are:

$$Q = \begin{pmatrix} 300 \cdot I_3 & O_3 \\ O_3 & 3 \cdot I_3 \end{pmatrix}; R = 2 \cdot I_3$$

$$K = \begin{pmatrix} 12.247 & 0 & 0 & 1.909 & 0 & 0 \\ 0 & 12.247 & 0 & 0 & 1.418 & 0 \\ 0 & 0 & 12.247 & 0 & 0 & 1.251 \end{pmatrix}$$

$$\begin{pmatrix} 12.247 & 0 & 0 & 1.909 & 0 & 0 \\ 0 & 12.247 & 0 & 0 & 1.251 \end{pmatrix}$$

$$\begin{pmatrix} 12.247 & 0 & 0 & 1.418 & 0 \\ 0 & 0 & 12.247 & 0 & 0 & 1.251 \end{pmatrix}$$

$$\begin{pmatrix} 12.247 & 0 & 0 & 1.418 & 0 \\ 0 & 0 & 1.251 & 0 & 1.251 \end{pmatrix}$$

$$\begin{pmatrix} 13.247 & 0 & 0 & 1.418 & 0 \\ 0 & 0 & 1.251 & 0 & 1.251 \end{pmatrix}$$

$$\begin{pmatrix} 13.247 & 0 & 0 & 1.418 & 0 \\ 0 & 0 & 1.251 & 0 & 1.251 \end{pmatrix}$$

$$\begin{pmatrix} 13.247 & 0 & 0 & 1.418 & 0 \\ 0 & 0 & 1.251 & 0 & 1.251 \end{pmatrix}$$

$$\begin{pmatrix} 13.247 & 0 & 0 & 1.418 & 0 \\ 0 & 0 & 1.251 & 0 & 1.251 \\ 0.15 & 0.15 & 0.15 & 0.25 \\ 0.15 & 0.15 & 0.25 \\ 0.15 & 0.15 & 0.25 \\ 0.15 & 0.15 & 0.25 \\ 0.15 & 0.15 & 0.25 \\ 0.15 & 0.15 & 0.25 \\ 0.15 & 0.15 & 0.25 \\ 0.15 & 0.15 & 0.25 \\ 0.15 & 0.15 & 0.25 \\ 0.15 & 0.15 & 0.25 \\ 0.15 & 0.15 & 0.25 \\ 0.15 & 0.15 & 0.25 \\ 0.15 & 0.15 & 0.25 \\ 0.15 & 0.15 & 0.25 \\ 0.15 & 0.15 & 0.25 \\ 0.15 & 0.15 & 0.25 \\ 0.15 & 0.15 & 0.25 \\ 0.15 & 0.15 & 0.25 \\ 0.15 & 0.15 & 0.25 \\ 0.15 & 0.25 & 0.25 \\ 0.15$$

Figure 3: State and reference tracking under IJC.

This control strategy provided accurate tracking for most of the states, with fast convergence and minimal overshoot. Once the corresponding feedback gain *K* was obtained, the same controller was applied to the original nonlinear model. The results confirm that the control law remained effective, with the system maintaining stability and accurate trajectory tracking despite the presence of nonlinearities.

The state responses obtained using the LQR are illustrated in Figure 4. The state trajectories are plotted in blue, while the position reference signals are in red. The IJC results show slower responses compared to the LQR. All states converge to the reference, with no overshoot and no steady state error, confirming the effectiveness of the LQR design. The settling times for each joint are about 0.47 sec for x_1 , 0.43 sec for x_2 , and 0.46 sec for x_3 .

After the LQR design, the next step was to compute the observer gain L, based on the pole placement. Specifically, the poles of the closed-loop system with the state-feedback controller were multiplied by a factor of 2 in magnitude. This pole placement strategy ensures that the observer responds relatively quickly to any deviations between the measured and estimated outputs. Excessively fast poles would increase estimation speed but also demand high sampling rates and computational power, which may not be feasible in a low-cost implementation. The chosen configuration ensures estimation while reliable state maintaining compatibility with practical hardware constraints.

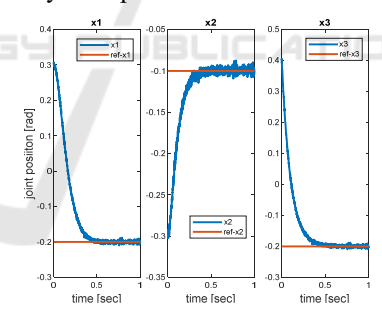


Figure 4: LQR-State trajectories and position reference.

As a result, the final poles of the observer are $p = 10^2 \cdot [-9.07; -1.15; -0.20; -0.20; -0.21; 0.09i; -0.21 + 0.09i]$. The gain observer matrix is:

$$L = 10^{3} \cdot \begin{pmatrix} 0.033 & 0.047 & -0.651 \\ 0.086 & 0.098 & 0.574 \\ 0.068 & 0 & 0.975 \\ 0.111 & 0.886 & -15.659 \\ 1.852 & 1.610 & 13.841 \\ 1.399 & 0.001 & 19.564 \end{pmatrix}$$
(21)

The results using the LQR controller together with the Luenberger state observer are presented in Figure 6. The same feedback gain *K*, as a full state LQR, was used with the same initial conditions.

In Figure 5, the positions (x_1, x_2, x_3) are plotted in blue, the corresponding estimated states are shown in red (coincide with the estimated states), and the reference signals are displayed in magenta. The simulation results show that the positions successfully converge to the reference values without steady-state error, and that the estimated states match the true states, confirming the effectiveness of the overall controller-observer structure. The closed-loop performance achieved using the LQR controller in combination with the Luenberger observer demonstrates accuracy across all controlled joints. The settling times are approximately 0.46 sec for x_1 , 0.41 sec for x_2 , and 0.47 sec for x_3 . Throughout the simulation, none of the joint responses exhibited overshoot or steady-state error.

The estimation error $(x - x_e)$ generated by the Luenberger observer is on the order of 10^{-2} . The estimation error in all state components converges toward zero. Figure 6 shows the control signals for the three joints under each control strategy: the IJC command is shown in red, the LQR command in blue, and the LQR with observer in magenta (considered best result in terms of noise reduction), with the last two overlapping almost entirely. All signals remain within the $\pm 10 \, Nm$ range, which represents the considered torque limit for the actuators.

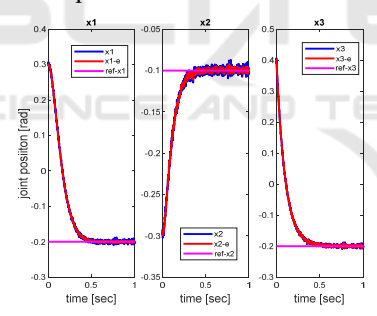


Figure 5: System and estimated states and reference trajectories for Luenberger observer.

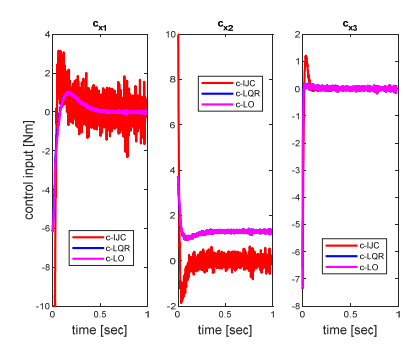


Figure 6: Control signals for the system with the IJC, LQR controller and LQR with Luenberger observer.

The IJC method stands out for its simplicity and ease of implementation, providing fast response for joint x_3 . However, it shows a significant overshoot for x_2 and a small steady-state position error for x_3 , highlighting the limitations of decoupled control.

The LQR achieves excellent overall performance, with fast convergence, no overshoot, and zero steady-state error, but it relies on full state feedback, which may not be feasible in low-cost implementations.

In contrast, the LQR controller combined with a Luenberger observer maintains similar performance levels while using only joint position measurements. This approach proves effective not only in reducing sensor requirements but also in dealing with modelling uncertainties and measurement noise, making it highly suitable for practical, low-cost rehabilitation systems.

5 CONCLUSIONS

This work presents the design, modeling, and control simulation of a wrist rehabilitation robot developed from scratch with emphasis on simplicity, low cost, and compactness. The device is intended to support repetitive wrist rehabilitation exercises, and to serve as a practical solution for both clinical and homebased rehabilitation.

Three control strategies were implemented in simulation: IJC, LQR, and an observer-based LQR. All proved feasible within the robot's simplified structure and intended use. IJC offers a straightforward and accessible approach, while LQR provides superior tracking accuracy and disturbance rejection. The observer-enhanced LQR further increases practicality by relying only on position sensors, reducing hardware requirements while maintaining performance.

These results establish a foundation for selecting suitable control methods depending on application priorities such as simplicity, precision, or sensor economy. The findings will guide prototype development, including the choice of motors, sensors, and embedded hardware. They also highlight the trade-offs between ease of implementation (IJC), high control performance (LQR), and cost efficiency (LQR + Observer). The next step is to build the physical prototype and perform real-time testing, initially with healthy users and later with patients under clinical supervision.

Future work will expand the system's capabilities by including additional degrees of freedom and modeling human-robot interaction forces to better mimic realistic therapy. Integrating physiological feedback, such as electromyographic (EMG) signals, could enable adaptive control strategies that adjust to patient effort and fatigue. Long-term clinical studies with healthcare professionals will also be pursued to evaluate therapeutic outcomes and refine rehabilitation protocols. Overall, the proposed system demonstrates strong potential for becoming an affordable and effective rehabilitation tool suitable for deployment in hospitals and home-based recovery programs.

ACKNOWLEDGEMENTS

This research was supported by the project New frontiers in adaptive modular robotics for patient-centered medical rehabilitation—ASKLEPIOS, funded by European Union—NextGenerationEU and Romanian Government, under National Recovery and Resilience Plan for Romania, contract no. 760071/23.05.2023, code CF 121/15.11.2022, with Romanian Ministry of Research, Innovation and Digitalization, within Component 9, investment 18.

REFERENCES

- Akdogan, E. (2016). Upper limb rehabilitation robot for physical therapy: design, control, and testing. *Turkish Journal of Electrical Engineering and Computer Sciences*, 24(3), 911-934.
- Basteris, A., et al (2014). Training modalities in robot-mediated upper limb rehabilitation in stroke: a framework for classification based on a systematic review. *J Neuroeng Rehabil*, 11 111. doi:10.1186/1743-0003-11-111
- Franklin, G., Powell, J. D., & Emami-Naeini, A. (2014). Feedback Control Of Dynamic Systems (7th ed.). Prentice Hall Press.
- Guozheng, X., et al (2014). Clinical experimental research on adaptive robot-aided therapy control methods for upper-limb rehabilitation. *Robotica*, 32(7), 1081–1100.
- Krebs, H., et al (1999). Overview of clinical trials with MIT-MANUS: a robot-aided neuro-rehabilitation facility. *Technology and Health Care*, 419-423.
- Levine, W. S. (2011). The Control Systems Handbook: Control System Advanced Methods (2nd ed). CRC Press.
- Major, Z. Z., et al (2021). Comparative Assessment of Robotic versus Classical Physical Therapy Using Muscle Strength and Ranges of Motion Testing in Neurological Diseases. *Journal of Personalized Medicine*, 11(10), 953.
- Masiero, S., Armani, M., & Giulio, R. (2011). Upper-limb robot-assisted therapy in rehabilitation of acute stroke patients: Focused review and results of new randomized

- controlled trial. *Journal of Rehabilitation Research and Development*, 48(4), 355-366.
- Mehrez, O., et al (2025). Development of an exoskeleton for wrist-joint rehabilitation: modeling, identification, and control. *Multibody System Dynamics*. doi:10.1007/s11044-025-10066-0
- Omarkulov, N., et al (2016). Preliminary mechanical design of NU-Wrist: A 3-DOF self-aligning Wrist rehabilitation robot. 2016 6th IEEE International Conference on Biomedical Robotics and Biomechatronics (BioRob), (pp. 962-967). Singapore.
- Parisi, A., et al (2022). Efficacy of Multisensory Technology in Post-Stroke Cognitive Rehabilitation: A Systematic Review. *Journal of Clinical Medicine*, 11(21), 6324.
- Pollock, A., et al (2014). Interventions for improving upper limb function after stroke. *Cochrane Database of Systematic Reviews*, 11(1).
- Prewett, M. S., et al (2010). Managing workload in humanrobot interaction: A review of empirical studies. Computers in Human Behavior, 26(5), 840-856.
- Rosati, G., Gallina, P., & Masiero, S. (2007). Design, Implementation and Clinical Tests of a Wire-Based Robot for Neurorehabilitation. *IEEE Trans. on Neural Systems and Rehabilitation Eng.*, 15(4), 560-569.
- Spong, M. W., Hutchinson, S., & Vidyasagar, M. (2005). Robot Modeling and Control (First ed.), Wiley.
- Squeri, V., et al (2014). Wrist rehabilitation in chronic stroke patients by means of adaptive, progressive robotaided therapy. *IEEE Transactions on Neural Systems and Rehabilitation Engineering*, 22(2), 312-325.
- Tarnita, D., et al (2022). Analysis of Dynamic Behavior of ParReEx Robot Used in Upper Limb Rehabilitation. Applied Sciences, 12(15), 7907.
- Tohanean, N., et al (2023). The Efficacity of the NeuroAssist Robotic System for Motor Rehabilitation of the Upper Limb—Promising Results from a Pilot Study. Journal of Clinical Medicine, 12(2), 425.
- Toth, A., et al (2005). Passive robotic movement therapy of the spastic hemiparetic arm with REHAROB: report of the first clinical test and the follow-up system improvement. 9th International Conference on Rehabilitation Robotics, 127-130. Chicago, IL, USA.
- Tucan, P., et al (2022) Design and Experimental Setup of a Robotic Medical Instrument for Brachytherapy in Non-Resectable Liver Tumors. Cancers 2022, 14, 5841. https://doi.org/10.3390/cancers14235841
- Vaida C., et al (2018) Innovative development of a spherical parallel robot for upper limb rehabilitation. Int. J. Mech. Robot. Syst. 2018;4:256. doi: 10.1504/IJMRS.2018.096302.
- Wu, C., et al (2011). Randomized Trial of Distributed Constraint-Induced Therapy Versus Bilateral Arm Training for the Rehabilitation of Upper-Limb Motor Control and Function After Stroke. *Neurorehabilitation & Neural Repair*, 25(2), 130-139.